A. DI GERLANDO, R. PERINI

MODELLING AND EXPERIMENTAL ANALYSIS OF CORE SATURATION AND LOSSES OF UNIVERSAL MOTORS

INTERNATIONAL CONFERENCE
ON ELECTRICAL MACHINES
ICEM 2002

Conference Record on CD
Paper N° 090

Brugge, Belgium, 25-28 August 2002


Conference Record
ICEM 2002
15th International Conference on Electrical Machines
Old St. Jan Conference Centre, Brugge, Belgium, August 25-28, 2002
Editors:
R. Belmans (KU Leuven) and J. Melkebeek (Ghent University)

Modelling and Experimental Analysis of Core Saturation and Losses of Universal Motors

A. Di Gerlando, R. Perini

Dipartimento di Elettrotecnica – Politecnico di Milano
Piazza Leonardo da Vinci 32, I – 20133 Milano, Italy
phone: +39 02 23993722 (14) – fax: +39 02 23993703 - e-mails: [antonino.digerlando, roberto.perini]@polimi.it

***Abstract* — With the intent to model the global behaviour of the universal motor, taking into account core saturation and losses, an equivalent circuit of the machine is described.**
A procedure for the calculation of the magnetisation characteristic is developed, correctly modelling the armature reaction; a speed-dependent core losses lumped conductance is evaluated. Simulated and test results validate the model.

1. Introduction

The commutator universal motor (UM), whose operation principle and main characteristics are well known, is still largely used in several small rating home and commercial appliances: nevertheless, the increasing competition of other solutions leads to deepen the knowledge of this machine, both in order to attain design improvements, and to allow a more accurate estimate of its performances [1-10].

Among the aspects that significantly affect the operation, the ferromagnetic core behaviour is to be noted: the high and non uniform level of saturation, together with the double frequency rotor lamination losses, make not negligible the core non linear effects, especially in high speed motors (running at some ten thousands RPM).

The core saturation affects both the global operating quantities (particularly current and torque waveforms), and the commutation parameters (especially self and mutual inductances of the commutating sections).

The paper is devoted to model the global operation of the motor: to this aim, the following steps are considered:
– an equivalent circuit is presented, including saturation;
– the magnetisation characteristic is analytically obtained;
– the core loss and the derived conductance are evaluated;
– results of FEM simulations and tests validate the model.

2. Equivalent circuit

The reference motor data are in Table I. Called $m_f = N_f \cdot i_m$ the field magnetizing m.m.f., in the generic position ζ under the upper pole of fig.1, the total m.m.f. $m_p(\zeta)$ equals:

$$m_p(\zeta) = m_f \cdot (1 + \sigma \cdot (\zeta - \alpha)),\ \sigma = (N_a / N_f) / (2 \cdot \pi); \quad (1)$$

σ (reaction factor) and α (equivalent brush shifting) take into account the distorting and demagnetizing effects of the armature m.m.f. reaction (slot stepping neglected in (1)).
As shown later, for given values of σ and α, (1) leads to evaluate the magnetisation characteristic $\varphi_m(m_f)$, linking the instantaneous values of the pole flux φ_m and of the field winding m.m.f. m_f: for low m_f levels, $\varphi_m(m_f)$ reduces to the unsaturated curve $\varphi_{mo} = \Lambda_o \cdot m_f$.
By the Faraday's law, the armature flux linkage leads to the total e.m.f. e_a, as measured at the brushes: it consists of e_{at} and e_{as}, transformer and speed e.m.f.s respectively:

$$e_a = e_{at} + e_{as} = C_{at} \cdot N_a \cdot \frac{d\varphi_m}{dt} + C_{as} \cdot N_a \cdot \varphi_m \cdot \Omega\ , \quad (2)$$

with C_{at} and C_{as} linkage coefficients (dependent on ε, α; for the motor of Table 1, we have: $C_{at} = -0.059$; $C_{as} = 0.31$).

By defining $$\Lambda_a = \varphi_m / m_f \quad (3)$$

$$\Lambda_d = d\varphi_m / dm_f \quad (4)$$

apparent and differential permeances, (2) becomes:

$$e_a = e_{at} + e_{as} = L_{da}(i_m) \cdot di_m/dt + M(i_m) \cdot i_m \cdot \Omega \quad (5)$$

where $$L_{da}(i_m) = N_a \cdot N_f \cdot C_{at} \cdot \Lambda_d(i_m) \quad (6)$$

and $$M(i_m) = N_a \cdot N_f \cdot C_{as} \cdot \Lambda_a(i_m)\ . \quad (7)$$

The e.m.f. induced in the two field coils is given by:

$$e_f = 2 \cdot N_f \cdot d\varphi_m/dt = L_{df}(i_m) \cdot di_m/dt\ , \quad (8)$$

with $$L_{df}(i_m) = 2 \cdot N_f^2 \cdot \Lambda_d(i_m)\ . \quad (9)$$

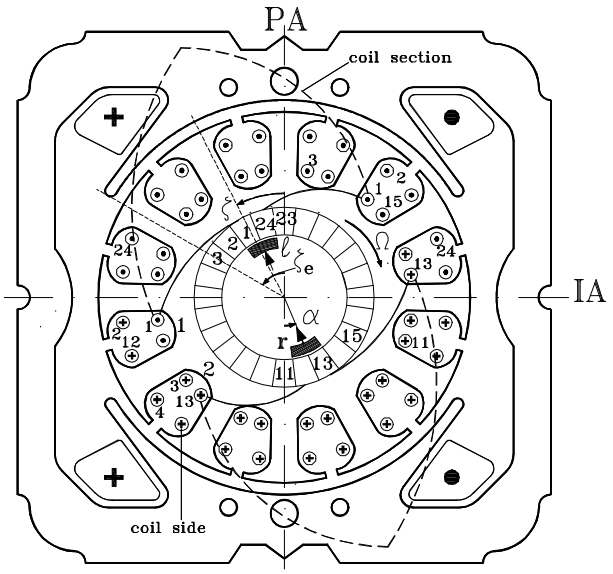

Fig.1. Scheme of the reference universal motor.

TABLE I
MAIN QUANTITIES OF THE REFERENCE UNIVERSAL MOTOR

V_n [V]; I_n [A]; P_{in} n [W]	220; 5.8; 1250
f_n [Hz]; N_n [r.p.m.]	50; 32,000
N° of poles p; N° of commutator segments k	2; 24
N° of rotor teeth N_t; coil sides/(layer-slot): u	12; 2
rotor winding paths: a=p; pole shoe extension $2 \cdot \zeta_e$	2; 2·60°
Rotor turns N°: N_a; wire diameter [mm]	360; 0.40
field coil turns N° (per pole): N_f; wire diam. [mm]	130; 0.63
turn pitch shortening: ε; equiv. brush shifting: α	30°; 22.5°
Brush sizes: $w_b \cdot \ell_b \cdot h_b$ [mm]	6.3 · 10.95 · 37
brush–segments contact ratio; rotor diam. [mm]	1.96; 38.25
air gap δ; axial stack length ℓ_s; lam. width [mm]	1.47; 32; 0.50
lam.AST FEV 4750: nom. loss 1.5T, 50Hz [W/kg]	4.7

Besides the e.m.f.s induced by the flux φ_m, the model must include: inductive voltage drops (due to $L_{\ell f}$, $L_{\ell a}$: leakage field and armature inductances); resistive voltage drops (due to field and armature resistances R_f and R_a and to the brushes, $v_b \approx R_b \cdot i_m$); as regards the core losses, they can be modelled by a suited conductance G_c, derived at the input terminals.
Thus, by some handling and parameter combinations, the equivalent circuit of fig.2 can be derived, where:

$$R = R_f + R_a + R_b \ , \qquad (10)$$

$$L(i_m) = L_{df}(i_m) + L_{da}(i_m) + L_{\ell f} + L_{\ell a} \ . \qquad (11)$$

About the electromagnetic torque $T_e(i_m)$, it is expressed by:

$$T_e(i_m) = M(i_m) \cdot i_m^2 \ . \qquad (12)$$

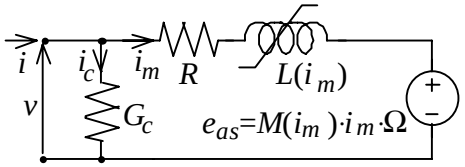

Fig.2. Equivalent circuit of the universal motor.

The circuit of fig.2 is valid for the analysis of every kind of operating condition. Some of its parameters (e.g.: winding resistances and leakage inductances) are quite easily valuable, while the magnetisation characteristic $\varphi_m(m_f)$ and the core loss conductance G_c require a detailed analysis.

3. Magnetisation Characteristic Calculation

In UMs, magnetic saturation is important in the leading pole tips, in the rotor teeth faced to them and in the yokes. Thus, the air-gap magnetic voltage $U_\delta(\zeta)$ is notably lower than the m.m.f $m_p(\zeta)$, requiring a correct evaluation of the ferromagnetic voltage drops: for each current i_m, the corresponding flux φ_m is computed by iterations as follows:
- a pole axis-tooth axis rotor alignment is chosen (fig.3);
- the pole flux fringing is considered by extending the pole tips of a width equal to one air-gap at each extreme;
- the slotting is taken into account by the Carter's factor;
- $U_\delta^{(k)}(\zeta)$ is the $U_\delta(\zeta)$ distribution at the kth iteration;
- $U_\delta^{(0)}(\zeta)$ is assumed a fraction x of $m_p(\zeta)$ (e.g. $x = 0.50$);
- within the pole arc, the elementary air-gap flux equals:

$$d\varphi_\delta(\zeta) = U_\delta^{(k)}(\zeta) \cdot d\Lambda_\delta(\zeta) \ , \qquad (13)$$

with $d\Lambda_\delta(\zeta)$ elementary air-gap magnetic permeance;
- then, the pole flux φ_m is given by:

$$\varphi_m^{(k)} = \int_{\zeta=-\zeta_e}^{\zeta=\zeta_e} d\varphi_\delta(\zeta) \ ; \qquad (14)$$

- the flux $\varphi_{pt}^{(k)}(\zeta)$ crossing the generic section of the saturated pole tip (the left one in fig. 3) equals:

$$\varphi_{pt}^{(k)}(\zeta) = \int_{\zeta=\zeta_e}^{\zeta} d\varphi_\delta(\zeta) \ ; \qquad (15)$$

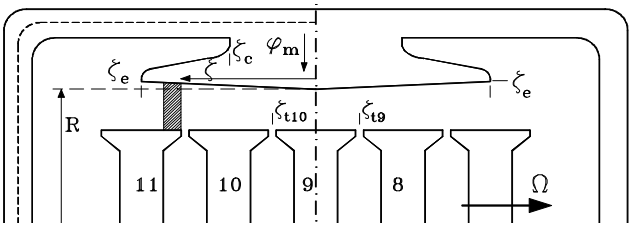

Fig. 3 - Scheme of the magnetic structure used for the analytical evaluation of the magnetisation characteristic.

- the flux density $B_{pt}^{(k)}(\zeta)$ along the pole tip is given by:

$$B_{pt}^{(k)}(\zeta) = \varphi_{pt}^{(k)}(\zeta) / A_{pt}(\zeta) \ , \qquad (16)$$

with $A_{pt}(\zeta)$ cross section of the pole tip in position ζ;
- from the lamination $H_{fe}(B)$ curve, the $H_{pt}^{(k)}(\zeta)$ follows:

$$H_{pt}^{(k)}(\zeta) = H_{fe}\left(B_{pt}^{(k)}(\zeta)\right); \qquad (17)$$

- the magnetic voltage drop $U_{pt}^{(k)}$, measured from the external edge of the leading pole tip, equals:

$$U_{pt}^{(k)}(\zeta) = \int_{\zeta=\zeta_e}^{\zeta} H_{pt}^{(k)}(\zeta) \cdot (r_s \cdot d\zeta) \ , \qquad (18)$$

with r_s stator internal radius along the pole shoe;
- the magnetic voltage drops along the pole body and the trailing pole tip are negligible for usual current values;
- the stator yoke magnetic voltage drop is globally evaluated, assuming uniform flux density in the cross section;
- the tooth magnetic voltage drop is evaluated singly, considering each tooth flux and the flux crossing the slots;
- as for the rotor yoke magnetic voltage, an equivalent length is assumed (3/8 of the geometrical length);
- the various voltage drops are locally summed, thus giving the k-th step reconstructed m.m.f. distribution $m_{pr}^{(k)}(\zeta)$;
- then the air-gap magnetic voltage is updated as follows:

$$U_\delta^{(k+1)}(\zeta) = U_\delta^{(k)}(\zeta) \cdot \left(m_p(\zeta) / m_{pr}^{(k)}(\zeta)\right)^\Delta \ , \qquad (19)$$

where Δ is a relaxation exponent, necessary to obtain the numerical convergence (a suited Δ value equals $\Delta \approx 0.25$);
- the iterative process continues until the reconstructed m.m.f. distribution at the kth iteration, $m_{pr}^{(k)}(\zeta)$, equals the impressed one, $m_p(\zeta)$, unless a chosen difference.

For each current value, a diagram of the magnetic voltage drop distributions is obtained: fig.4 shows these drops for i_m=10 A, together with $m_p(\zeta)$, all referred to the m.m.f. m_f.

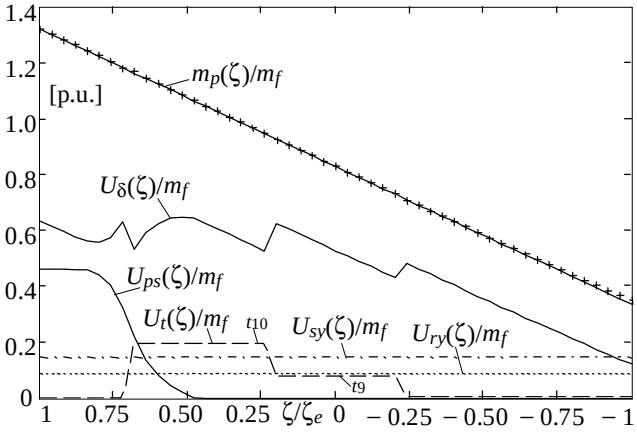

Fig. 4 – Pole m.m.f. $m_p(\zeta)$ and magnetic voltage drops under the pole shoe, referred to m_f (data: Table I; i_m = 10 A ≈ peak saturated value of I_n): air gap (U_δ/m_f), rotor teeth (t_9, t_{10}: see fig.3) (U_t/m_f), pole shoe (U_{ps}/m_f), yokes (U_{sy}/m_f, U_{ry}/m_f); + = $m_{pr}^{(20)}(\zeta)/m_f$.

It can be observed that:
- the air-gap magnetic voltage drop U_δ behaves similarly to m_f : thus, the ratio U_δ/m_f is fairly constant; the irregular waveform of U_δ is due to the slotting effect;
- the voltage drop in the leading pole tip U_{ps} is relevant;
- the teeth drops U_t under the leading pole tip are high;
- U_{sy} and U_{ry} are notable: moreover, they are constant, i.e. ζ independent, because they are not air-gap distributions.

To obtain the magnetisation characteristic, the described procedure must be repeated for several current values.

Fig.5 shows the characteristic obtained by the described analytical method (—), together with the curve derived by FEM analyses (---), up to very high peak current values (I_{mpMax} = 40 A, typical of zero speed starting at full voltage); some measurement points are also reported (o), obtained by using a probe coil placed on the pole shoe tips.
The initial permeance Λ_o of the unsaturated portion of the characteristic ($\varphi_{mo} = \Lambda_o \cdot m_f$) equals Λ_o = 0.92 μH.
The agreement is satisfactory, thus validating the analytical method, significantly quicker than the FEM analysis.

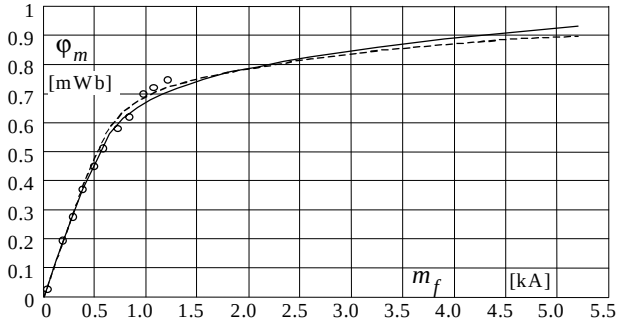

Fig.5. Magnetisation characteristic evaluated by analytical calculation (—), FEM analysis (---) and tests (o) (motor data: Table I)

FEM analysis has also shown that, for each current value, the pole flux is practically independent on the rotor position (see Table II), having considered the different slot current distributions. This pole flux invariance (that justifies the (tooth axis) – (pole axis) disposition adopted by the analytical method) is due to the designed extension of the pole shoe, in relation to the rotor teeth disposition: this leads to a constant air-gap pole permeance, thus limiting undesirable effects (torque ripple and flux pulsations).

TABLE II
RATIOS OF FEM EVALUATED POLE FLUXES (AT VARIOUS MMF.S): TOOTH AXIS-POLE AXIS ALIGNMENT (φ_{mt}); SLOT AXIS-POLE AXIS ALIGN. (φ_{ms})

m_f [kA]	0.13	0.65	1.30	2.60	5.20
φ_{mt} / φ_{ms}	0.998	0.997	1.006	1.016	1.019

4. Core Loss Modelling

As known, the accurate evaluation of the core losses of rotating electrical machines is still a challenge: besides the basic non-linearities of the classical core losses, the occurrence of other loss items (rotational hysteresis, extra losses) make very complex and specialised the experimental and FEM research activities in this field [11].

Here, just the classical core losses in steady-state periodic operation are considered, distinguished in specific eddy (p_e) and hysteresis losses (p_h). As shown in § 3, in the UM the spatial distribution of the air-gap flux density is not sinusoidal (thus implying a distorted distribution in the core portions too: see fig.6); moreover, in case of converter feeding, also the pole flux time waveform is distorted. Thus, in order to correctly estimate the core losses, the effects of the space and time harmonics must be included.
The following steps will be considered: parameter extraction of the specific core losses from the lamination manufacturer test data; evaluation of the local loss items, as a function of position and time, considering the double frequency rotor magnetisation; definition and estimation of space and time harmonic loss coefficients, suited to give the actual core losses from the core losses evaluated on the basis of space and time fundamental sinusoidal waveforms; evaluation of the core loss equivalent conductance G_c.
From the lamination tests, performed with sinusoidal flux density waveform, the following expression of the specific core loss $p_{c\$}$ [W/kg] has been obtained (average loss/cycle):

$$p_{c\$} = p_{e\$} \cdot \hat{B}^2 \cdot (f / f_o)^2 + p_{ho}(\hat{B}) \cdot (f / f_o), \qquad (20)$$

with $$p_{ho}(\hat{B}) = p_{ha} \cdot \hat{B}^a + p_{hb} \cdot \hat{B}^b \quad ; \qquad (21)$$

f_o=50 Hz: $p_{e\$}$=0.54; p_{ha}=0.95; p_{hb}=0.30; a=1.18; b=4.00.
In case of non sinusoidal, periodic magnetisation $b(t)$ with period $T = 1/f$ (without minor hysteresis loops), the hysteresis loss item remains unvaried (with $\hat{B}$ peak instantaneous value), while the average eddy loss p_e over T equals:

$$p_e = k_e \cdot \frac{1}{T} \cdot \int_0^T (db(t)/dt)^2 \, dt \; ; \qquad (22)$$

the use of (22) in sinusoidal operation allows to obtain k_e:

$$k_e = p_{e\$} / (2 \cdot \pi^2 \cdot f_o^2) \; . \qquad (23)$$

The UM portions considered for the core loss evaluation are stator yoke (s), rotor teeth (t) and rotor yoke (y): some core losses occur also in pole shoes and in teeth heads, but they will be neglected, due to the small masses involved.
The stator loss evaluation is quite simple (because each stator particle, fixed in space, is subjected to a magnetisation at line frequency $f_\ell = 1/T_\ell$): it will be performed later.
Conversely, the rotor loss is less easy to be estimated, due to the magnetisation at the internal frequency f_i, superposed to that at frequency f_ℓ: it will be analysed in detail.
Consider the following expression of the space and time dependence of the flux density distribution b in the rotor:

$$b = B(\xi) \cdot \upsilon(t) \; , \qquad (24)$$

where: ξ = generic angular rotor position (measured as ζ, see fig.1); $\upsilon(t)$ = time dependence of the flux density distribution inside the rotor: $\upsilon(t)$, that is proportional to the pole flux time waveform $\varphi_m(t)$, has a peak value equal to $\hat{\upsilon}$.
In case of sinusoidal voltage feeding, $\upsilon(t)$ can be assumed sinusoidal (in fact, the waveform distortion, due to saturation, is typical of $i_m(t)$, while $\varphi_m(t)$ remains practically sinusoidal); on the contrary, in general (e.g., in case of converter feeding, [8]) $\upsilon(t)$ is just periodic: $\upsilon(t) = \upsilon(t + T_\ell)$.
As concerns $B(\xi)$, it can be regarded in two different ways:
– we can follow the magnetic events of each rotor particle, during its rotation (lagrangian viewpoint): $B = B(\xi(t))$: in this case, according to the verses of fig.1, we have:

$$-d\xi/dt = \Omega = \omega_i \cdot 2/p = 2 \cdot \pi \cdot f_i \cdot 2/p = 2 \cdot \pi \cdot f_i \; ; \qquad (25)$$

– we can consider the flux density distribution in all the rotor simultaneously, by observing all the fixed positions ξ=ζ, covered by different rotor particles during rotation (eulerian viewpoint): B=$B(\zeta)$; moreover: $B(\zeta)$= $B(\zeta + 2\cdot\pi)$.

According to the lagrangian viewpoint, the local instantaneous specific eddy loss $p_{e\xi t}$, in each tooth or yoke rotor particle, moving with motion law $\xi(t)$, equals:

$$p_{e\xi t}(\xi(t), \upsilon(t)) = k_e \cdot (db/dt)^2 = k_e \cdot \{d[B(\xi(t)) \cdot \upsilon(t)]/dt\}^2 \qquad (26)$$

$$\Rightarrow \; p_{e\xi t}(\xi, t) = k_e \cdot \left\{ [(dB/d\xi) \cdot \omega_i \cdot \upsilon]^2 + [(d\upsilon/dt) \cdot B]^2 + \right. \\ \left. - 2 \cdot \omega_i \cdot B \cdot (dB/d\xi) \cdot \upsilon \cdot (d\upsilon/dt) \right\} \; . \qquad (27)$$

Now consider the eulerian viewpoint of a stationary observer, that examines the instantaneous specific rotor core loss in each fixed position: this corresponds to pose ζ instead of ξ in (27), leading to $p_{e\zeta t}(\zeta,t)$. In order to obtain the instantaneous eddy global loss in each rotor homogeneous portion (teeth or yoke), it is convenient to evaluate a space average value $p_{et}(t)$ of $p_{e\zeta t}(\zeta,t)$:

$$p_{et}(t) = \frac{1}{2\cdot\pi}\cdot\int_0^{2\cdot\pi} p_{e\zeta t}(\zeta,t)\cdot d\zeta \ ; \qquad (28)$$

thanks to the fact that the application of (28) to the third term of (27) gives zero, from (28) it follows:

$$p_{et}(t) = p_{eti} + p_{et\ell} = k_e\cdot\left(I_i\cdot\omega_i^2\cdot\upsilon^2(t) + I_\ell\cdot(d\upsilon/dt)^2\right), \qquad (29)$$

$$I_i = \frac{1}{2\cdot\pi}\cdot\int_0^{2\cdot\pi}\left(\frac{dB(\zeta)}{d\zeta}\right)^2 d\zeta \ ; \ I_\ell = \frac{1}{2\cdot\pi}\cdot\int_0^{2\cdot\pi} B(\zeta)^2\, d\zeta \ . \qquad (30)$$

Both $B(\zeta)$ and $\upsilon(t)$ can be expressed as a Fourier series:

$$B(\zeta) = \sum_{n=1}^{\infty}\hat{B}_n\cdot\cos(n\cdot\zeta + \vartheta_{Bn}) \qquad (31)$$

$$\upsilon(t) = Y_0 + \cos(\omega_\ell\cdot t) + \sum_{z>1}^{\infty} Y_z\cdot\cos(z\cdot\omega_\ell\cdot t + \vartheta_{\upsilon z}) \ . \qquad (32)$$

(31) and (32) include all the possible operating situations:

- $B(\zeta)$ is surely non sinusoidal, with zero average value;
- as regards $\upsilon(t)$, various conditions can occur: with constant d.c. voltage feeding, just the average value Y_0 exists; in case of sinusoidal voltage feeding, just the fundamental harmonic exists; if an a.c. converter voltage feeding is provided (TRIAC, a.c. chopper), $\upsilon(t)$ contains the first and the higher order odd harmonics, without Y_0; finally, in case of d.c. chopper, Y_0 is included.

The substitution of (31) in (30) gives:

$$I_i = \beta_i\cdot\left(\hat{B}_1^2/2\right) \qquad I_\ell = \beta_\ell\cdot\left(\hat{B}_1^2/2\right) \ , \qquad (33)$$

$$\text{with } \beta_i = \sum_{n=1}^{\infty}\left(n\cdot\hat{B}_n/\hat{B}_1\right)^2 \ , \quad \beta_\ell = \sum_{n=1}^{\infty}\left(\hat{B}_n/\hat{B}_1\right)^2 \ ; \qquad (34)$$

β_i and β_ℓ can be called eddy space harmonic factors: they would reduce to unity in the ideal case of a purely sinusoidal distribution of the flux density in the rotor portions.

About $\upsilon(t)$, in the following, the presence of a constant d.c. component Y_0 will be excluded (anyway, it would correspond to a classical rotor core loss component, easily valuable); we suppose the existence of the fundamental harmonic of $\upsilon(t)$; thus, from (29) and (32), the time average specific rotor eddy losses, in the period T_ℓ equals:

$$p_e = \frac{1}{T_\ell}\int_0^{T_\ell} p_{et}(t)dt = p_{ei} + p_{e\ell} = k_e\left(J_i I_i\omega_i^2 + J_\ell I_\ell\right), \qquad (35)$$

$$\text{with } J_i = \frac{1}{T_\ell}\int_0^{T_\ell}\upsilon^2(t)dt = \frac{1}{2}\left(1 + \sum_{z>1}^{\infty} Y_z^2\right) = \frac{1+\Re_i}{2}, \qquad (36)$$

$$J_\ell = \frac{\int_0^{T_\ell}\left(\frac{d\upsilon}{dt}\right)^2 dt}{T_\ell} = \omega_\ell^2\,\frac{1+\sum_{z>1}^{\infty}(z\cdot Y_z)^2}{2} = \omega_\ell^2\cdot\frac{1+\Re_\ell}{2}. \qquad (37)$$

$\Re_i$ and $\Re_\ell$, that can be called time harmonic coefficients, represent the effects of the time harmonics on the rotor eddy losses: thus, they are zero in case of sinusoidal $\upsilon(t)$.

On the basis of (23), (33)-(37), the specific rotor eddy losses due to the internal and line frequencies become:

$$p_e = p_{e\$}\cdot\hat{B}_1^2\cdot\left(\frac{1+\Re_i}{2}\cdot\beta_i\cdot\left(\frac{f_i}{f_o}\right)^2 + \frac{1+\Re_\ell}{2}\cdot\beta_\ell\cdot\left(\frac{f_\ell}{f_o}\right)^2\right) \qquad (38)$$

In the ideal case ($\Re = 0$; $\beta = 1$), (38) shows a factor ½, absent in the first term of (20): ½ is due to the space average value of the rotor squared fundamental component of $B(\zeta)$.

The rotor hysteresis losses should be estimated in a similar manner, but here no instantaneous loss can be defined: hence, only the space-time average value p_h in the period T_ℓ can be considered. Accepting the superposition principle of the losses occurring at the f_ℓ and f_i frequencies, we have:

$$p_h = p_{h\ell} + p_{hi} \ . \qquad (39)$$

The first term $p_{h\ell}$, existing even at zero speed, equals:

$$p_{h\ell} = \frac{1}{2\cdot\pi}\cdot\int_0^{2\cdot\pi} p_{ho}\left(\left|B(\zeta)\cdot\hat{\upsilon}\right|\right)\cdot d\zeta\cdot(f_\ell/f_o). \qquad (40)$$

As regards the second term of (39), during the rotation each rotor particle is cyclically magnetised, at frequency f_i, between quasi symmetrical peak flux density values, slowly modulated according to $\upsilon(t)$. A reasonable approximation of this phenomenon consists in evaluating an instantaneous hysteresis loss $p_{hit}(t)$, considered constant in each period T_i:

$$p_{hit}(t) = p_{ho}\left(\left|\hat{b}(t)\right|\right)\cdot(f_i/f_o) = p_{ho}\left(\left|\hat{B}\cdot\upsilon(t)\right|\right)\cdot(f_i/f_o), \qquad (41)$$

with $\hat{B} = B(\zeta_p)$ peak flux density of the space distribution, occurring inside the rotor portion, in the fixed position ζ_p.

The average hysteresis specific loss at frequency f_i equals:

$$p_{hi} = \frac{1}{T_\ell}\int_0^{T_\ell} p_{hit}(t)dt = \frac{1}{T_\ell}\int_0^{T_\ell} p_{ho}\left(\left|\hat{B}\cdot\upsilon(t)\right|\right)\cdot dt\cdot\frac{f_i}{f_o}. \qquad (42)$$

$$\text{By posing:} \qquad \gamma_i = \hat{B}/\hat{B}_1 \ , \qquad (43)$$

and considering (21), (42) can be transformed as follows:

$$p_{hi} = \left(\eta_a\, p_{ha}\cdot\gamma_i^a\cdot\hat{B}_1^a + \eta_b\, p_{hb}\cdot\gamma_i^b\cdot\hat{B}_1^b\right)\cdot(f_i/f_o), \qquad (44)$$

$$\text{where} \qquad \eta_\nu = \int_0^{T_\ell}|\upsilon(t)|^\nu\, dt\Big/T_\ell, \quad \text{with } \nu = a, b \ . \qquad (45)$$

η_a and η_b can be called hysteresis modulation factors; in case of sinusoidal $\upsilon(t)$, we have: $\eta_a = 0.61$; $\eta_b = 0.38$.

The specific rotor loss expressions (38) and (39) show that:

- at zero speed just $p_{h\ell}$ exist, while near the rated speed the losses p_{hi} are prevailing, considering that $f_{in} > 10\cdot f_\ell$;
- the space harmonic effects are included in β_i, β_ℓ, and γ_i, while the time harmonics affect $\Re_i$, $\Re_\ell$, η_a and η_b: their evaluation allows to calculate the average rotor specific losses, once known the space fundamental flux density;
- as known, the space distribution $B(\zeta)$ depends on saturation, that apparently affects also β_i, β_ℓ, and γ_i;
- on the other hand, by combining (30) and (33), it follows:

$$\beta_i = \frac{1}{\pi\hat{B}_1^2}\int_0^{2\cdot\pi}\left(\frac{dB(\zeta)}{d\zeta}\right)^2 d\zeta = \frac{1}{\pi}\int_0^{2\cdot\pi}\left(\frac{d}{d\zeta}(\underline{b}(\zeta))\right)^2 d\zeta \qquad (46)$$

$$\beta_\ell = \left(1/\pi\hat{B}_1^2\right)\cdot\int_0^{2\cdot\pi} B^2(\zeta)d\zeta = \frac{1}{\pi}\int_0^{2\cdot\pi}(\underline{b}(\zeta))^2\, d\zeta \qquad (47)$$

$$\text{with} \qquad \underline{b}(\zeta) = B(\zeta)/\hat{B}_1 \ ; \qquad (48)$$

it follows that, even if $B(\zeta)$, $\hat{B}$ and $\hat{B}_1$ deeply depend on saturation when evaluated separately, their ratio $\underline{b}(\zeta)$ and γ_i can be considered less saturation dependent; hence:

- m_f amplitude does not affect $\underline{b}(\zeta)$ and γ_i: thus, β_i, β_ℓ, γ_i can be estimated with $m_f = 1$, neglecting the saturation;
- conversely, the saturation must be correctly considered in evaluating the fundamental flux density component;
- about $p_{h\ell}$, its manipulation is more complex; however, this term becomes negligible at usual operating speeds.

Fig.6 shows the p.u. flux density distributions $\underline{b}_t(\zeta)$ and $\underline{b}_y(\zeta)$ in the rotor teeth and yoke of the motor of Table I (actual values divided by the corresponding fundamental amplitudes); also the air-gap flux density $\underline{b}_\delta(\zeta)$ is reported (referred to teeth fundamental flux density too).

These distributions have been evaluated analytically from (1), neglecting saturation and pole tip fringing: thus, $\underline{b}_\delta(\zeta)$ presents discontinuities at the pole tip edges. On the contrary, $\underline{b}_t(\zeta)$ changes smoothly: in fact, the tooth flux density has been evaluated in terms of space moving average of the $\underline{b}_\delta(\zeta)$ distribution, in one tooth pitch $\zeta_t = 2\cdot\pi/N_t$:

$$\underline{b}_t(\zeta) = \frac{1}{\zeta_t}\cdot\int_{\zeta_1}^{\zeta_2}\underline{b}_\delta(x)dx \ , \quad \zeta_1 = \zeta - \frac{\zeta_t}{2} \ , \ \zeta_2 = \zeta + \frac{\zeta_t}{2} \ ; \quad (49)$$

this implies a gradual $\underline{b}_t(\zeta)$ transition at the pole shoe tips.

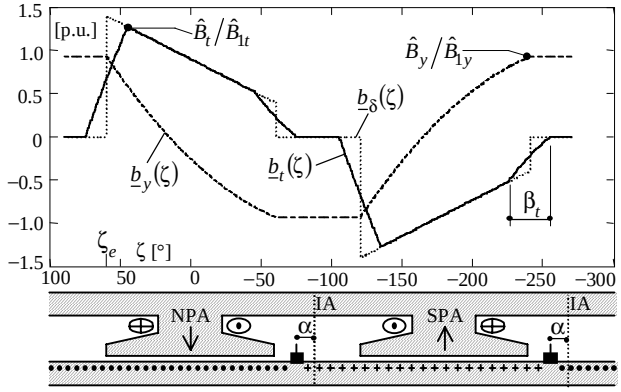

Fig.6. Flux density p.u. distributions $\underline{b}_t(\zeta)$, $\underline{b}_y(\zeta)$ in rotor teeth and yoke (actual values divided by the corresponding fundamental amplitudes; motor of Table I); p.u. air-gap flux density $\underline{b}_\delta(\zeta)$ (referred to teeth fundamental flux density): analytical evaluation; saturation and fringing neglected (PA, IA= polar, interpolar axis).

The analytical formulation of $\underline{b}_t(\zeta)$ and $\underline{b}_y(\zeta)$ has led to obtain the following closed-form expressions of the teeth and yoke space factors, dependent on α, σ, ζ_e and ζ_t: their values are given in Table III, for the motor of Table I.

$$\beta_{it} := \frac{\frac{\pi}{16}\cdot\zeta_t\cdot\left[\left[\sigma^2\cdot\left(\alpha^2+\zeta_e{}^2-\frac{\zeta_t{}^2}{6}\right)+1\right]-2\cdot\sigma\cdot\alpha\right]}{\sin\left(\frac{1}{2}\cdot\zeta_t\right)^2\cdot\left[\sin(\zeta_e)^2\cdot(1-\sigma\cdot\alpha)^2+\sigma^2\cdot\left(\zeta_e{}^2\cdot\cos(\zeta_e)^2-\zeta_e\cdot\sin(2\cdot\zeta_e)+\sin(\zeta_e)^2\right)\right]} \quad (50)$$

$$\beta_{et} := \frac{1}{64}\cdot\frac{\left[\frac{2}{3}\cdot\frac{\left[(1-\sigma\cdot\alpha)^2\cdot(6\cdot\zeta_e-\zeta_t)+\sigma^2\cdot\zeta_e{}^2\cdot(2\cdot\zeta_e-\zeta_t)\right]}{\pi}+\frac{1}{30}\cdot\sigma^2\cdot\frac{\zeta_t{}^3}{\pi}\right]}{\left[\sin\left(\frac{1}{2}\cdot\zeta_t\right)^2\cdot\left[\sin(\zeta_e)^2\cdot(1-\sigma\cdot\alpha)^2+\sigma^2\cdot\left(\zeta_e\cdot\cos(\zeta_e)-\sin(\zeta_e)\right)^2\right]\right]}\cdot\pi^2\cdot\zeta_t{}^2 \quad (51)$$

$$\gamma_{it} := \pi\cdot\zeta_t\cdot\frac{\left[1+\sigma\cdot\left(\zeta_e-\frac{\zeta_t}{2}-\alpha\right)\right]}{8\cdot\sin\left(\frac{\zeta_t}{2}\right)\cdot\sqrt{\sigma^2\cdot\left(\cos(\zeta_e)\cdot\zeta_e-\sin(\zeta_e)\right)^2+\sin(\zeta_e)^2\cdot(1-\sigma\cdot\alpha)^2}} \quad (52)$$

$$\beta_{iy} := \frac{\pi}{12}\cdot\zeta_e\cdot\frac{\left[3\cdot(1-\sigma\cdot\alpha)^2+\sigma^2\cdot\zeta_e{}^2\right]}{\left[\sigma^2\cdot\left(\cos(\zeta_e)\cdot\zeta_e-\sin(\zeta_e)\right)^2+\sin(\zeta_e)^2\cdot(1-\sigma\cdot\alpha)^2\right]} \quad (53)$$

$$\beta_{ey} := \frac{\left[\left[(1-\sigma\cdot\alpha)^2\cdot\zeta_e{}^2\cdot\left(\frac{\pi}{2}-\zeta_e\right)\right]+\left[\frac{\zeta_e{}^3}{3}\cdot(1-\sigma\cdot\alpha)^2+\frac{2}{15}\cdot\sigma^2\cdot\zeta_e{}^5\right]\right]}{4\cdot\left[\sigma^2\cdot\frac{\left(\cos(\zeta_e)\cdot\zeta_e-\sin(\zeta_e)\right)^2}{\pi}+\sin(\zeta_e)^2\cdot\frac{(1-\sigma\cdot\alpha)^2}{\pi}\right]} \quad (54)$$

$$\gamma_{iy} := \frac{(1-\sigma\cdot\alpha)\cdot\zeta_e}{\frac{4}{\pi}\cdot\sqrt{\sigma^2\cdot\left(\cos(\zeta_e)\cdot\zeta_e-\sin(\zeta_e)\right)^2+\sin(\zeta_e)^2\cdot(1-\sigma\cdot\alpha)^2}} \ . \quad (55)$$

The numerical results of Table III suggest some remarks:

– the tooth eddy loss factor β_{it} appears very high: this is due to the $\underline{b}_t(\zeta)$ slopes at the tip edges in (46); these slopes are linked to the intense eddy currents occurring in each tooth core during its entry and exit under the pole field;
– also the yoke eddy factor β_{iy} is due to the $\underline{b}_y(\zeta)$ slopes, but the space filtering effect due to the teeth distributed flux contributions make more smoothed the $\underline{b}_y(\zeta)$ slopes;
– as regards $\beta_{\ell t}$ and $\beta_{\ell y}$, (47) shows that they represent the squared value of the space r.m.s. p.u. flux density: thus, observing $\underline{b}_t(\zeta)$ and $\underline{b}_y(\zeta)$, it is reasonable that $\beta_{\ell t} > \beta_{\ell y}$;
– the values of γ_{it} and γ_{iy} come from (43) and fig.6; in fact:

$$\hat{B}_t = \gamma_{it}\cdot\hat{B}_{1t} > \hat{B}_{1t} \ ; \qquad \hat{B}_y = \gamma_{iy}\cdot\hat{B}_{1y} < \hat{B}_{1y} \ . \quad (56)$$

TABLE III
VALUES OF THE ROTOR TEETH (t) AND YOKE (y) SPACE FACTORS, EVALUATED ANALYTICALLY BY (50)-(55) (MOTOR DATA: TABLE I)

$\beta_{it} = 2.54$ $\beta_{\ell t} = 1.07$ $\gamma_{it} = 1.27$	$\beta_{iy} = 1.16$ $\beta_{\ell y} = 1.01$ $\gamma_{iy} = 0.93$

The estimation of the actual core losses is based on the assumption that the flux density waveform $b_q(t)$ (in the equivalent section area A_q of each core portion; $q = s, t, y$) is proportional to the pole flux $\varphi_m(t)$ waveform (as already assumed in (24) for the time dependence of the flux density distribution); thus, for each motor portion, we can write:

$$b_q(t) = \varphi_m(t)/A_q \ , \qquad q = s, t, y \ , \quad (57)$$

$$\hat{B}_{1q} = \hat{\Phi}_{m1}/A_q \ , \qquad q = s, t, y \ , \quad (58)$$

in time domain and for the time fundamental harmonics.

Eq.(57) is not obvious, because the different local saturation levels could imply a non perfect proportionality link among the local flux density $b_q(t)$ and the global flux $\varphi_m(t)$: a few FEM and circuit simulations have shown that (57) is acceptably satisfied in all the magnetic branches.

The equivalent sections A_q and the masses M_q equal:

$$A_s = 2\cdot w_{ys}\cdot k_{st}\cdot\ell_s \ , \qquad M_s = \rho_{fe}\cdot A_{es}\cdot h_{ys} \ , \quad (59)$$

$$A_t = \frac{2}{\pi}\cdot\frac{N_t}{p}\cdot w_t\cdot k_{st}\cdot\ell_s \ , \quad M_t = \rho_{fe}\cdot N_t\cdot w_t\cdot h_t\cdot k_{st}\cdot\ell_s \ , \quad (60)$$

$$A_y = 2\cdot w_{yr}\cdot k_{st}\cdot\ell_s \ , \quad M_y = \rho_{fe}\cdot w_{yr}\cdot k_{st}\cdot\ell_s\cdot\pi\cdot D_{yr} \ , \quad (61)$$

with k_{st} stacking factor, w (h) width (height) of the considered branch, D_{yr} average yoke diameter, ρ_{fe} core density; thus, the core losses can be evaluated as follows:

$$P_c = P_{cs} + P_{ct} + P_{cy} = \sum_{q=s,t,y} M_q\cdot\left(p_{eq}+p_{hq}\right) \ . \quad (62)$$

The stator specific losses are given by:

$$p_{es} = p_{e\$}\cdot\hat{B}_{1s}^2\cdot\left(1+\Re_\ell\right)\cdot\left(f_\ell/f_o\right)^2 \quad (63)$$

$$p_{hs} = \left(p_{ha}\cdot\hat{B}_{1s}^a\cdot\hat{\upsilon}^a + p_{hb}\cdot\hat{B}_{1s}^b\cdot\hat{\upsilon}^b\right)\cdot\left(f_\ell/f_o\right), \quad (64)$$

while the specific eddy and hysteresis losses in rotor teeth and yoke can be evaluated by (38) and (44), once inserted the appropriate peak flux densities (from (58), with q = t, y) and the space and time harmonic coefficients.

By (58) and (62), the core losses can be written as follows:

$$P_c = P_c\left(\hat{\Phi}_{m1}, f_\ell, f_i\right) \ ; \quad (65)$$

in (65) the space harmonic factors are known quantities for a given motor, while the time harmonic factors ($\Re_i$, $\Re_\ell$, η_a, η_b) must be evaluated from the actual $\varphi_m(t)$ waveform.

Now consider the sinusoidal feeding operation at $f_\ell = f_n$ ($\rightarrow \varphi_m(t)$ roughly sinusoidal): for a fixed rms value V of $v(t)$, the internal frequency and the peak pole flux depend on the rotational speed only; thus, (65) becomes:

$$P_c = P_c(V,\Omega) \ ; \qquad (66)$$

the core loss estimation for the motor of Table I at rated voltage and speed gives: $P_{cn} = P_c(V_n, \Omega_n) = 30$ W.

Fig.7 shows the p.u. core loss dependence on the p.u. speed, for a few voltage rms p.u. values around the rated condition. From (66), the following derived conductance G_c can be defined at the input terminals of the fig.2 circuit:

$$G_c(V,\Omega) = P_c(V,\Omega) / V^2 \ , \qquad (67)$$

whose p.u. curves are shown in fig.8: the spread of the values confirms the heavy non-linear nature of the core behaviour, both concerning magnetisation and losses.

Even if no direct experimental core losses measurements were possible, some indirect evaluations have shown the soundness of the obtained results.

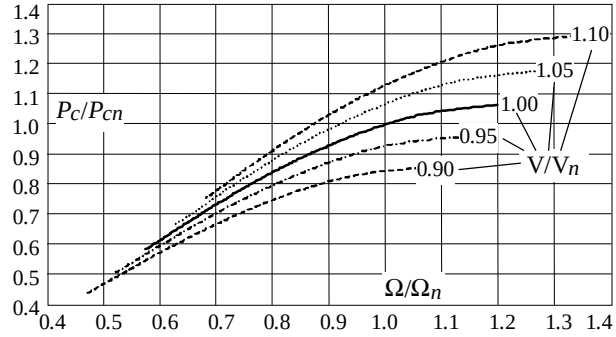

Fig.7. Estimated p.u. core losses, as a function of the p.u. speed, with rms p.u. voltage as a parameter, for the motor of Table I, fed by sinusoidal voltage at f_ℓ = 50 Hz ($P_{cn} = P_c(V_n, \Omega_n) = 30$ W).

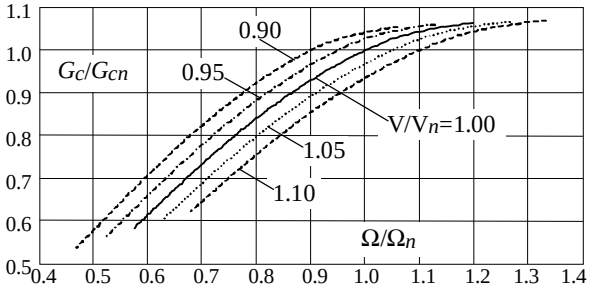

Fig.8. Estimated p.u. equivalent conductance (see fig.2), as a function of the p.u. speed, with rms p.u. voltage as a parameter (motor data: Table I; $G_{cn} = G_c(V_n, \Omega_n) = P_{cn} / V_n^2$).

As an example of the global correctness of the developed model, fig.9 shows the waveform of the simulated and of the measured input current $i(t)$, for the motor of Table I, under rated voltage feeding, while fig.10 illustrates the rms value of the input current as a function of the speed, under rated voltage too: a fair agreement can be recognised.

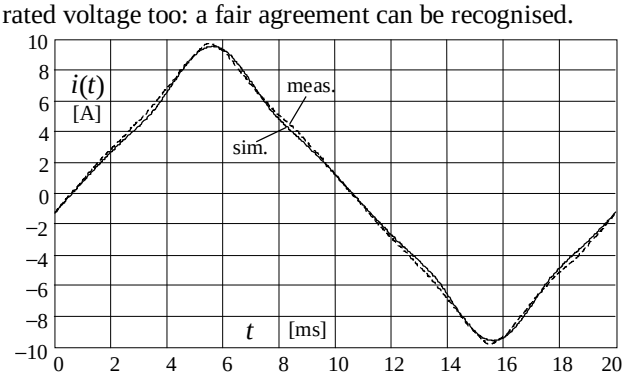

Fig.9. Waveform of input current $i(t)$, for the motor of Table I operating in rated conditions: simulated (—); measured (---).

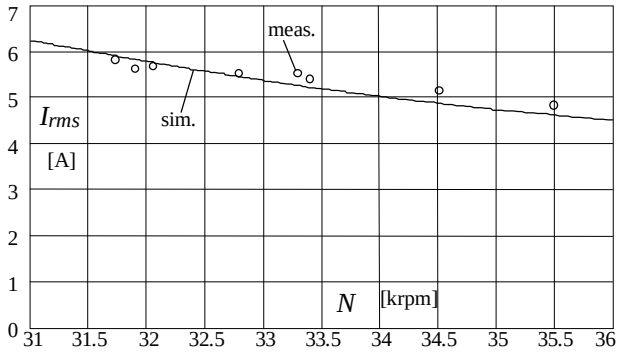

Fig.10. Input rms current as a function of the rotational speed: circuit simulation (—); tests (o) (motor data: Tab.I, rated feeding).

5. Conclusions

The paper has developed a model for the analysis of the global operation of the universal motor, with particular reference to the non-linear core behaviour:

- an equivalent circuit has been presented, including saturation effects, valid in general operating conditions;
- then, an analytical determination of the magnetisation characteristic has been performed, whose results have been validated with measurements and FEM simulations;
- subsequently, the stator and rotor core losses have been evaluated, considering saturation effects and space and time harmonics; hence, a lumped conductance has been obtained, as a function of voltage and speed;
- experimental results concerning a commercial motor have shown the soundness of the model.

Acknowledgement

Work financed by the Italian National Ministry of Education, University and Research (MIUR), Cofin 2001, Title: "Improvement of the energy efficiency of electrical motors and drives for industrial and civil applications".

References

[1] T. Fujii, "Study of UMs with lag angle brushes", *IEEE Trans. on PAS*, Vol. PAS-101, n° 6 June 1982.

[2] K. J. Bradley, W. M. H. Ismail, "The performance analysis of the single-phase, a.c. commutator motor", *5th Intern. IEE Conf. on Electrical Machines and Drives*, Session 5B, paper n° 3, London 1991.

[3] T. Matsuda et al., "Method for analysing the commutation in small UMs", *IEE Proc. on Electr. Power Appl.* Vol. 142, n° 2 March 1995.

[4] H. Wang Ren, R. Walter, "Computer aided simulation of performances and brush commutation for UMs with two coils per armature slot", *Intern. Conf. on Electric Machines and Drives IEMD '99*.

[5] T. McDermott et alii, "Electromechanical system simulation with models generated from FE solutions", *IEEE Tr. on Mag.*,v.33, 1997.

[6] M.C. Costa et alii, "Modified nodal analysis applied to electric circuits coupled with FEM in the simulation of UM", *ibidem*, v. 36, July 2000

[7] R. H. Wang, R. T. Walter, "Modeling of UM performance and brush commutation using FE computed inductance and resistance matrices", *IEEE Trans. on Energy Conversion*, Vol.15 Iss.3 , Sept. 2000.

[8] H. Bodur, A. F. Bakan, M. H. Sarul, "UM speed control with current controlled PWM AC chopper by using a microcontroller", *Proc. of IEEE Intern. Conf. on Industrial Technology*, Vol.1, 2000

[9] B. Bencdicic et alii, "Evolutionary optimization of a UM", *IECON '01: 27th IEEE Ind. Electr. Soc. Annual Meet.*, Vol.1, 2001

[10] J. Cros, P. Viarouge, Y. Chalifour, J. Figueroa, "A new structure of UM using soft magnetic composites", *36th IAS Meeting*, vol.1, 2001.

[11] J. G. Zhu, V. S. Ramsden, "Improved formulations for rotational core losses in rotating electrical machines", *IEEE Trans. on Mag, Vol.34, N.4*, July 1998.